Journal of Alloys and Compounds 509 (2011) 2986–2992

Contents lists available at ScienceDirect

Journal of Alloys and Compounds

journal homepage: www.elsevier.com/locate/jallcom

Effects of Ce^{3+} concentration, beam voltage and current on the cathodoluminescence intensity of SiO_2:Pr^{3+}–Ce^{3+} nanophosphor

G.H. Mhlongo[a,b], O.M. Ntwaeaborwa[b,*], M.S. Dhlamini[a], H.C. Swart[b], K.T. Hillie[a,b,**]

[a] National Centre for Nano-structured Materials, CSIR, PO Box 395, 1 Meiring Naude Road, Brummeria, Pretoria ZA0001, South Africa
[b] Department of Physics, University of the Free State, Bloemfontein ZA9300, South Africa

ARTICLE INFO

Article history:
Received 4 November 2010
Received in revised form
23 November 2010
Accepted 26 November 2010
Available online 3 December 2010

Keywords:
Cathodoluminescence
Energy transfer
Degradation

ABSTRACT

SiO_2:Pr^{3+}–Ce^{3+} phosphor powders were successfully prepared using a sol–gel process. The concentration of Pr^{3+} was fixed at 0.2 mol% while that of Ce^{3+} was varied in the range of 0.2–2 mol%. High resolution transmission electron microscopy (HRTEM) clearly showed nanoclusters of Pr and Ce present in the amorphous SiO_2 matrix, field emission scanning electron microscopy (FE-SEM) indicated that SiO_2 clustered nanoparticles from 20 to 120 nm were obtained. Si–O–Si asymmetric stretching was measured with Fourier transform-IR (FT-IR) spectroscopy and it was also realized that this band increased with incorporation of the activator ions into the SiO_2 matrix. The broad blue emission from the Ce^{3+} ions attributed to the $5d^1$–$4f^1$ transition was observed from the SiO_2:0.2 mol% Pr^{3+}–1 mol% Ce^{3+} phosphor. This emission was slightly enhanced compared to that of the singly doped SiO_2:1 mol%Ce^{3+} phosphor. Further investigations were conducted where the CL intensity was measured at different beam voltages and currents from 1 to 5 kV and 8.5 to 30 μA, respectively, in order to study their effects on the CL intensity of SiO_2:0.2 mol% Pr^{3+}–1 mol% Ce^{3+}. The electron-beam dissociated the SiO_2 and as a result an oxygen-deficient surface dead or non-luminescent layer of SiO_x, where $x < 2$ on the surface, was formed.

1. Introduction

Field emissive display (FED) technology is an excellent model for the next generation of display market due to its anticipated high brightness, high contrast ratio, light weight, and low-power consumption [1,2]. A phosphor layer serves as a crucial component on this display technology and most of the commercial FED phosphor layers (i.e. Y_2O_3:Eu^{3+} (red), $Y_3Al_5O_{12}$:Tb^{3+} (green), and Y_2SiO_3:Ce^{3+} (blue)) are rare earth based. Traditional sulphide phosphors for FEDs have demonstrated high luminous efficiency and high chromaticity [2]. However, they are still faced with one major challenge that their CL intensity degrade drastically under standard operating conditions (low voltage and high current densities) required for FEDs. It has been indicated that desorption of sulphur and formation of non-luminescent oxide layers on the surface takes place simultaneously with the CL intensity degradation [3]. Based on these findings, research focus has shifted to oxide phosphors which are emerging as possible candidates to replace traditional sulphide phosphors. The main reason for such interest on oxide phosphors is that they have demonstrated high thermal and thermodynamically stability [1]. Recently, red emitting $CaTiO_2$, $BaTi_4O_9$ and $SrTiO_3$ activated with Pr^{3+} phosphors were investigated for application in FEDs [2,4,5]. In addition, amorphous SiO_2 has been used as a host lattice for trivalent rare earth ions to prepare oxide based phosphors that could be used in low voltage FED technology. SiO_2 has emerged as a good host for rare earth ions due to its high transparency, chemical stability, dopant solubility and ease of production [6]. On the other hand, Lakshminarayana et al. [7] have recently incorporated Pr^{3+} in a transparent $KNbGeO_5$ nanocrystallized glass and studied its optical properties. These nanocrystalline glasses are also promising candidates for the study of nanostructures as they exhibited enhanced luminescence properties [7].

In this study, SiO_2:Ce^{3+}–Pr^{3+} powder phosphor was prepared using the sol–gel method. The concentration of Ce^{3+} was varied from 0.2 to 2 mol% while the Pr^{3+} concentration was fixed at 0.2 mol%. We also observed energy transfer from Pr^{3+} to Ce^{3+} which enhanced blue CL emission especially in the powders co-doped with 1 mol% of Ce^{3+} and 0.2 mol% of Pr^{3+}. The effects of varying the beam voltage and beam current were also investigated. Auger electron spectroscopy (AES) was used to monitor the surface chemical reactions taking place during prolonged electron bombardment.

1.1. Energy transfer between trivalent rare earth ions

There are four basic processes involved in energy transfer mechanisms between rare earth ions, namely (i) resonant radiative

* Corresponding author at: University of the Free State.
** Corresponding author at: National Centre for Nano-structured Materials, CSIR, PO Box 395, 1 Meiring Naude Road, Brummeria, Pretoria ZA0001, South Africa. Tel.: +27 12 841 3874; fax: +27 12 841 2229.
E-mail addresses: ntwaeab@ufs.ac.za (O.M. Ntwaeaborwa), thillie@csir.co.za (K.T. Hillie).

0925-8388/$ – see front matter © 2010 Elsevier B.V. All rights reserved.
doi:10.1016/j.jallcom.2010.11.179

transfer through emission of a sensitizer (S) and re-absorption by an activator (A); (ii) non-radiative transfer associated with resonance condition the energy absorber (sensitizer) and the emitter (acceptor); (iii) multiphonon assisted energy transfer; and (iv) cross-relaxation between two identical ions [8]. According to Zhang and Huang [8], the efficiency of radiative transfer relies on how efficiently the activator fluorescence is excited by the sensitizer emission. However, this requires a significant spectral overlap of the emission line of the sensitizer and the absorption line of the emitter. If the energy difference between the ground and excited states of the sensitizer is equal to that of acceptor and there exist a suitable interaction (i.e. multipolar and/or exchange interactions) between the ions, then energy transfer will most likely occur [9]. Exchange interaction of energy transfer may be responsible for near neighbours while the multipolar interaction usually governs interactions over separation of 20 Å between the donor and acceptor [9,10]. The basic theory of energy transfer has been established by several authors [6,8,9]. The rate of energy transfer between a donor and an acceptor derived by Dexter is as follows:

$$W_{DA} = 2\pi \left| \left\langle D, A^* \right| H_{DA} \left| D^*, A \right\rangle \right|^2 \int g_D(E) g_A(E) dE, \quad (1)$$

where D and A are the donor and acceptor, respectively. The integral denotes the spectral overlap between the donor emission and the acceptor absorption, the factors, $g_D(E)$ and $g_A(E)$ represent the normalized shape of the donor emission and acceptor absorption spectra, respectively while the matrix elements represents the wavefunction interaction between the initial state $\langle D, A^* |$ and the final state $|D, A^*\rangle$, and H_{DA} is the interaction Hamiltonian. The matrix elements can be expressed as a function of the donor and acceptor, so that the energy transfer probability depends upon the distance between the donor and acceptor.

If there is energy mismatch between the transitions of the donor and the acceptor especially if the transfer is between non-identical centres, the energy transfer processes needs to be assisted by lattice phonons and this process is called phonon-mediated energy transfer. In this energy transfer process, the electron-coupling together with the interaction (electric/magnetic multipolar) mechanisms responsible for the transfer must be taken into account [6]. It has been reported that for smaller energy mismatches, the transfer can be assisted by one or two lattice phonons [8]. However, energy mismatches as high as several thousand reciprocal centimetres have been encountered and this is higher than the Debye frequency normally found in host matrices, as a results multiphonon process is taken into considerations. Cross relaxation process on the other hand may give rise to the diffusion process already considered between sensitizers when the levels involved are identical or to self quenching when they are different. Since energy transfer in this study took place between two non-identical centres (i.e. ZnO and Pr^{3+}) and it is reasonable to speculate that the transfer was assisted by lattice phonons.

2. Experimental

SiO_2 co-doped with different concentrations of Pr^{3+}–Ce^{3+} ion pairs samples were prepared by mixing 0.05 mol of TEOS, 0.1 mol of H_2O, 0.1 mol of ethanol, and 0.145 mol of dilute nitric acid. The mixture was stirred at room temperature for 1 h to get a clear solution. Desired concentration of $Pr(NO)_3{\cdot}6H_2O$ dissolved in 5 ml of ethanol was added and the solution was stirred for 30 min. Finally, the desired amount of $Ce(NO)_3.6H_2O$ dissolved in 5 ml of ethanol was also added to the solution and stirred for another 30 minutes until a gel formed. The gel was then transferred to a petri dish for drying at room temperature for eight days and then annealed in air at 600 °C for 2 h.

The CL measurements were conducted using an Ocean Optics S2000 spectrometer attached to an ultra high vacuum chamber Physical Electronics PHI 549 Auger spectrometer. The first CL data were collected from the set of samples with different concentrations (0.2, 1, 1.5, and 2 mol%) of Ce^{3+} while the Pr^{3+} was fixed at 0.2 mol%. Further measurements were conducted from SiO_2:Pr^{3+} (0.2 mol%)–Ce^{3+} (1 mol%) whose CL intensity was comparatively the highest. The second set of CL data were recorded when the accelerating voltage was varied from 1 to 5 kV while keeping the beam current constant at 8.5 μA. The last sets of data were collected when the beam current was varied from 5 to 30 μA while the beam voltage was kept constant at 2 keV. The X-ray diffraction data were collected using X-ray diffractometer (Phillips Xpert) using a Cu Kα (λ = 1.5405 Å) radiation to study the crystal structure of the samples while the particle morphology and size were analysed using a JEOL JSM-7500F, Field Emission SEM and JEOL 2100, high resolution transmission electron microscopy (HRTEM). The chemical composition of the samples was analyzed using energy dispersive spectrometer (EDS). The Auger and CL data were simultaneously recorded from the PHI 549 Auger electron spectrometer (AES) and Ocean Optics S2000 Spectrometer. The phosphor powders were also irradiated with a beam of electrons (2 keV and beam current of 8.5 μA) under 1×10^{-7} Torr, O_2 pressure backfilled from a high vacuum base pressure of 1.2×10^{-8} Torr for several hours. The optical absorption properties of the samples were studied by a Spotlight 400 FTIR imaging system using the diffuse reflectance mode.

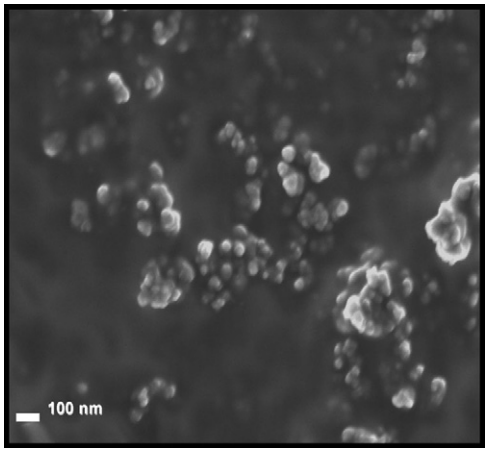

Fig. 1. FE-SEM image of the clustered SiO_2 nanoparticles calcined at 600 °C.

3. Results and discussion

The FESEM image in Fig. 1 illustrates the morphology of the SiO_2 nanoparticles calcined at 600 °C for 2 h. As shown in the image, the SiO_2 nanoparticles are clustered and are mostly spherical in shape with an average particle size in the range of ~20–120 nm in diameter. Similar images (not shown) were observed for SiO_2:Pr^{3+} and SiO_2:Pr^{3+}–Ce^{3+} as the added amounts of Pr^{3+} and/or Ce^{3+} ions did not affect the morphology.

EDS and HRTEM data confirmed the presence of rare earth clusters inside the silica matrix. As shown in Fig. 2(a), the HRTEM image revealed a high amorphous structure of SiO_2. This compares well with the XRD results (not shown). Fig. 2(a)–(c) present the HRTEM images of SiO_2 nanoparticles, SiO_2:Pr^{3+}, and SiO_2:Pr^{3+}–Ce^{3+}, respectively. From Fig. 2(b) and (c), it can be seen that black spots are uniformly dispersed in amorphous silica matrix. These were not observed in pure silica matrix as shown in Fig. 2(a). The chemical analyzes of the elemental present in the samples confirmed the presence of Si, O, Ce, and Pr as indicated in the EDS Fig. 2(d) and (e). Therefore based on these observations it was then concluded that the black spots represents clusters of rare earth ions with the size ranging from ~2 to 5 nm in diameter inside the SiO_2 matrix. These observations compares well with the results of Prakash et al. [11] and Fasoli et al. [12] where they observed clusters of Co doped $NiAl_2O_4$ in SiO_2, and Ce^{3+} in SiO_2, respectively.

Fig. 3 shows FTIR spectra of SiO_2, SiO_2:Pr^{3+}, SiO_2:Ce^{3+} and SiO_2:Pr^{3+}–Ce^{3+} all calcined at 600 °C for 2 h. The two absorption bands at 1160 and 1056 cm^{-1} corresponding to the LO and TO modes of Si–O–Si asymmetric stretching vibration (ν_{as}), respectively [13,14] were observed for all the samples. The weak absorption band at 945 cm^{-1} associated with Si–OH stretching mode was also present [13,14]. The presence of this absorption band can be due to the very strong Si–O–Si asymmetric stretching,

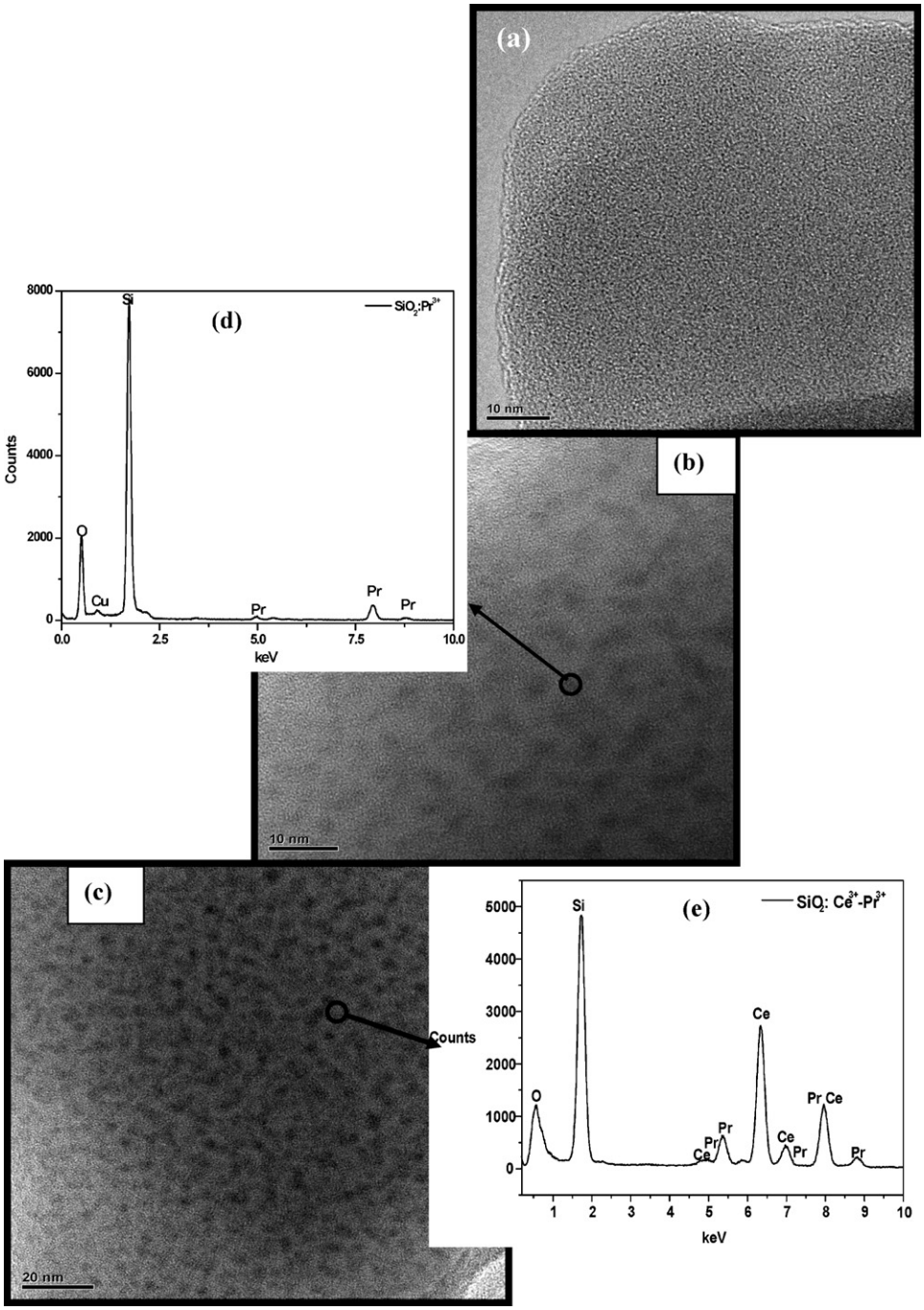

Fig. 2. HRTEM images and EDS spectra of (a) SiO_2 nanoparticles, SiO_2:Pr^{3+}, and (b) SiO_2:Pr^{3+}–Ce^{3+}.

ν_{as} (Si–O) absorptions in this region [13]. In addition, it was also realized that this band increased with incorporation of the activator ions into the SiO_2 matrix. Another absorption band associated with Si–O–Si symmetric stretching (ν_s) at 795 cm^{-1} was observed [13,14].

The CL emission spectrum of SiO_2 shown in Fig. 4 presents the broad emission band centred in the blue region at 445 nm which can be ascribed to either structural defects in the SiO_2 network or charge transfer between O and Si atoms [6]. The CL emission spectrum of the SiO_2:Ce^{3+} phosphor powders under irradiation of 2 keV electrons, 8.5 μA beam current in a high vacuum chamber at a base pressure of 1.2×10^{-8} Torr is shown in Fig. 5. The CL emission spectrum from SiO_2:Ce^{3+} consists of two blue bands located at 452 nm (weak) and 494 nm (strong). The peak positions were determined from Gaussian fits as clearly shown in the figure. The two bands at 452 nm and 494 nm can be associated with $^2D_{3/2}$–$^2F_{7/2}$ and $^2D_{3/2}$–$^2F_{5/2}$ of Ce^{3+}, respectively. Trivalent Ce ion has only one electron in the 4f state. The 4*f* electron of the $4f^1$ ground state configuration yields two components, $^2F_{5/2}$ and $^2F_{7/2}$ due to spin–orbit interaction and 5*d* electron of the excited $4f^0 5d^1$ configuration forms a ^2D term which is then split by crystal field into two stalk components, $^2D_{3/2}$ and $^2D_{5/2}$ states [6,15]. The CL emission spectra of the SiO_2:Pr^{3+}, SiO_2:Ce^{3+}, and SiO_2:Pr^{3+}–Ce^{3+} phosphor powders under irradiation with 2 keV electrons, 8.5 μA beam current in a high vacuum chamber at a base pressure of 1.2×10^{-8} Torr are shown in Fig. 6. The CL emission spectrum from

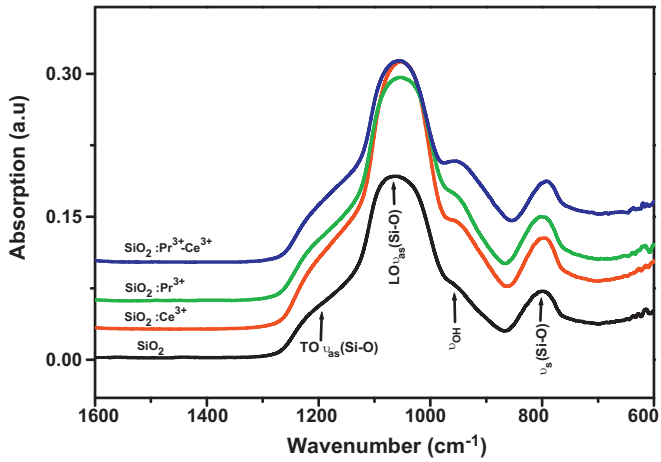

Fig. 3. FTIR absorption spectra of SiO_2, SiO_2:Pr^{3+}, SiO_2:Ce^{3+}, SiO_2:Pr^{3+}–Ce^{3+} phosphor powders.

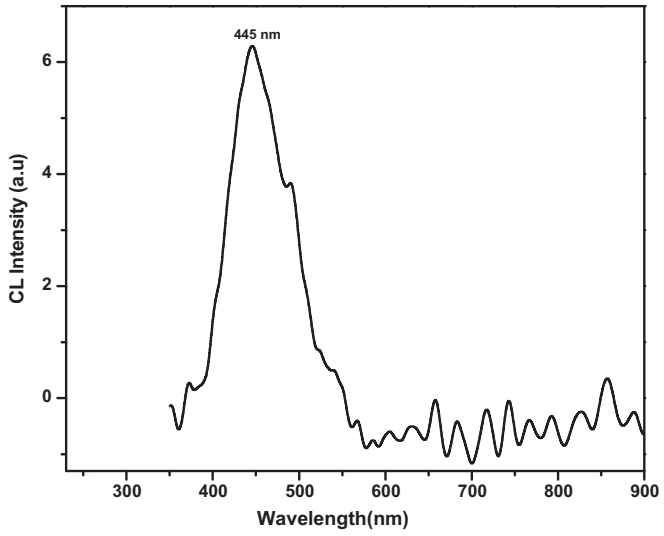

Fig. 4. CL emission spectra of SiO_2 nanoparticles irradiated with 2 keV, 8.5 μA beam of electrons in a high vacuum chamber containing 1.2×10^{-8} Torr.

SiO_2:Pr^{3+} showed the characteristic emission peaks of Pr^{3+} that can be associated with the transitions originating from the $^3P_0$ and $^1D_2$ multiplets to the $^3H_{(J=6,5,4)}$ and $^3F_{(J=2,3,4)}$ energy levels all localized in the $4f_2$ intra-configuration of the Pr^{3+} ions. The broad red emission

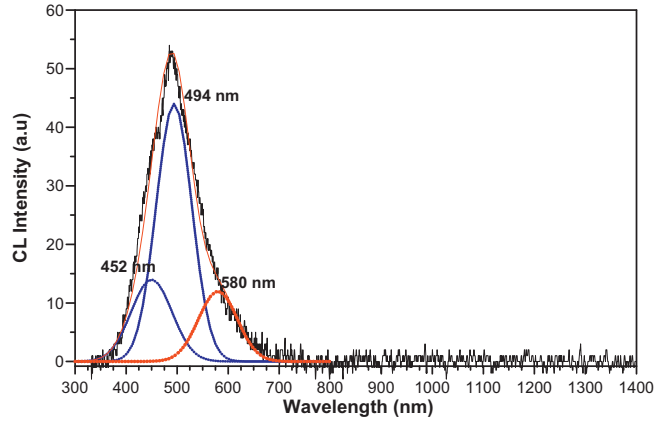

Fig. 5. CL emission spectrum of SiO_2:Ce^{3+} after irradiation with 2 kV, 8.5 μA beam of electrons in a high vacuum chamber containing a base pressure of 1.2×10^{-8} Torr.

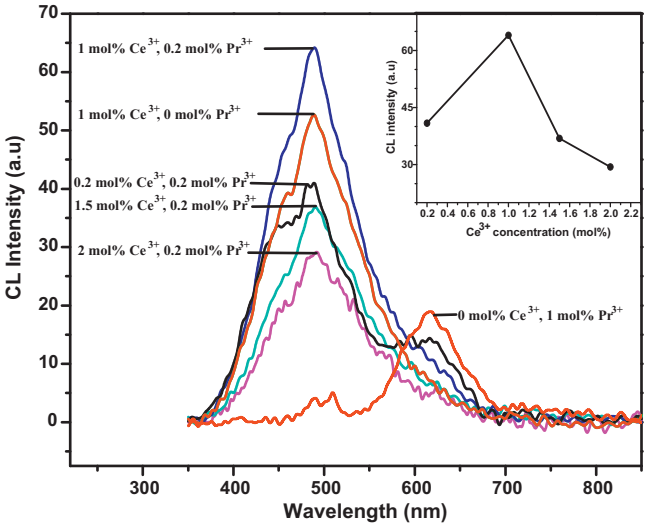

Fig. 6. CL emission spectra of the SiO_2:Pr^{3+} (1 mol%), SiO_2:Ce^{3+} (1 mol%), and SiO_2:Pr^{3+} (0.2 mol%)–Ce^{3+} (0.2, 1, 1.5, 2 mol%) irradiated with 2 kV, 8.5 μA beam of electrons in a high vacuum chamber containing a base pressure of 1.2×10^{-8} Torr. The insert shows the CL intensity as a function of different Ce^{3+} concentrations.

at 580–700 nm which could be due to both $^3P_0$–$^3H_6$ and $^1D_2$–$^3H_4$ transitions with dominant emission from $^3P_0$ level of Pr^{3+} was also observed (For interpretations of references to colour in Figs. 5 and 6, the reader is referred to the web version of this article.).

The CL emission spectra of SiO_2:Ce^{3+}–Pr^{3+} showed both bands from Ce^{3+} in the blue spectral region and a small shoulder from Pr^{3+} in the red spectral region when the amount of Pr^{3+} and Ce^{3+} were both 0.2 mol%. The small shoulder from Pr^{3+} was slowly quenched with increasing Ce^{3+} concentration and only blue emission from Ce^{3+} could be observed. Blue emission from Ce^{3+} was slightly enhanced with addition of 1 mol% Ce^{3+} into 0.2 mol% Pr^{3+} compared to singly doped SiO_2:Ce^{3+}. These results suggest the energy transfer from Pr^{3+} ions to its nearest neighbouring Ce^{3+} ions. The energy level diagram presented in Fig. 7 shows the energy transfer pathways between Pr^{3+} and Ce^{3+} ions. The main radiative transitions of Pr^{3+} and Ce^{3+} are designated with downward arrows. It appears that when the SiO_2:Ce^{3+}–Pr^{3+} phosphor is excited by 2 keV electrons, the excitation energy absorbed by Pr^{3+} ions promotes the electrons from the ground state $4f^2$ ($^3H_4$) to the excited $4f5d$ state of Pr^{3+} resulting in non-radiative relaxation from $4f5d$ state to $^3P_2$ level. This is followed by population of the $^3P_0$ by non-radiative decay from $^3P_2$ level as a result of consecutive radiative transitions in the orange ($^3P_0 \rightarrow {}^3H_4$) and red ($^3P_0 \rightarrow {}^3H_6$) regions with dominant emission from the $^3P_0 \rightarrow {}^3H_6$ transition. While the $^1D_2$ level is mainly populated by non-radiative relaxation from the $^3P_0$ which then leads to $^1D_2 \rightarrow {}^3H_4$ radiative transition in the red region. The non-radiation relaxation from $^1D_2$ to the $^1G_4$ is negligible due to the large band gap between these two levels, and hence the $^1G_4$ luminescence was not observed even for Pr^{3+} singly doped SiO_2. The quenching of broad red emission from Pr^{3+} centred at 614 nm with increasing Ce^{3+} concentration indicates that the energy transfer from Pr^{3+} to Ce^{3+} occurred faster than radiative processes of Pr^{3+} i.e. $^3P_0 \rightarrow {}^3H_6$ and $^1D_2 \rightarrow {}^3H_4$ which is only possible for nearest neighbouring ions in host matrix. This therefore means that the energy transfer from Pr^{3+} to Ce^{3+} occurred through the non-radiative relaxation from excited $4f\,^15d$ state to higher 3P level of Pr^{3+} ion to $5d$ state of Ce^{3+} ion, followed by the radiative relaxation of excited $5d$ electrons of Ce^{3+} ion. The quenching of luminescence with increasing Ce^{3+} ions may be due to formation of clusters of Ce^{3+} ions with Pr^{3+} in the host matrix. This could be due to self-quenching of Ce^{3+} neighbouring ions. At 1 mol% Ce^{3+}, the

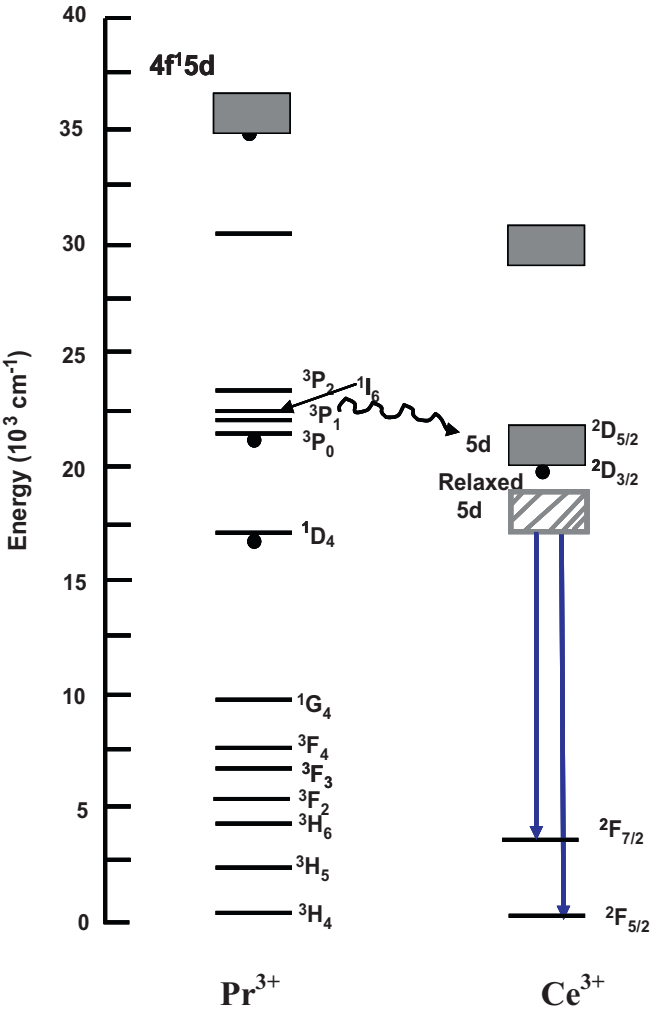

Fig. 7. Schematic energy level diagram showing the transition localized within Pr^{3+} and Ce^{3+} ions.

Ce^{3+} neighbouring ions may be near enough to transfer the energy from one to another. However, an increase in Ce^{3+} concentration led to the shortening of the distance between its neighbouring ions as a result of non-radiative loss of excitation energy between Ce^{3+} ions favouring quenching effect and decreasing luminescence intensity. Jang et al. [15] observed the energy transfer between Pr^{3+} and Ce^{3+}, as well as between Pr^{3+} and Tb^{3+} co-doped in $Y_3Al_5O_{12}$ (YAG). Nie et al. [16], on the other hand, reported the energy transfer between Pr^{3+} and Cr^{3+} in $SrAl_{12}O_{19}$. Vergeer et al. [17] and Meijerink et al. [18] found it difficult to find the efficient energy transfer from Pr^{3+} to Eu^{3+} irrespective of the fulfilment of an important condition for energy transfer which is the presence of resonance between Pr^{3+} and Eu^{3+} ions. The luminescence intensities were compared for different gels with and without Mg particles by varying the different concentrations of Mg [19]. Silica containing Mg^{2+} and Ce^{3+} ions had broad blue emission due to the energy transfer from Mg^{2+} to Ce^{3+}. An increase in luminescence intensity was observed as the Mg^{2+} to Ce^{3+} ratio increases for the range investigated.

The dependence of the CL intensity of SiO_2:Pr^{3+}–Ce^{3+} on different beam voltages from 1 to 5 kV while the beam current was fixed at 8.5 μA was investigated as shown in Fig. 8. When the beam current was fixed at 8.5 μA, the CL intensity of this phosphor increased upon increasing beam voltage from 1 to 5 kV. This indicates that saturation could not be reached up to 5 kV which is a good prospect for FEDs. Similarly, the CL intensity was observed to increase with an

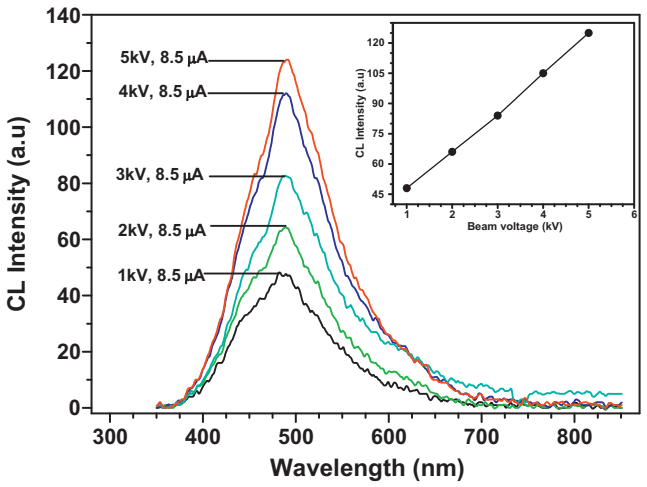

Fig. 8. CL emission intensities of Ce^{3+} in SiO_2: Pr^{3+}–Ce^{3+} phosphor as a function of different beam voltages.

increase in the beam current from 5 to 30 μA while the beam voltage was kept constant at 2 kV. Fig. 9 shows the beam current plotted against the maximum CL intensity of SiO_2:Pr^{3+}–Ce^{3+} at 488 nm. Again, no saturation was observed up to 30 μA. The increase of CL intensity with an increasing in beam voltage and beam current can be attributed to deeper penetration of electrons into the phosphor surface and the larger electron beam current density [20]. The electron penetration depth can be estimated using the following empirical formula:

$$L(\text{Å}) = 250(A/\rho)(E/Z^{1/2})^{n}, \quad (2)$$

where $n = 1.2/(1 - 0.29 \log_{10} Z)$, A represents the atomic weight of the material, ρ the density, Z is atomic number, and E is the accelerating beam voltage (kV) [20,21]. Fig. 10 shows the normalized calculated penetration depth plotted against the electron beam voltage. It can be clearly observed from this figure that the penetration of the energetic electrons into the phosphor was shown to increase with increasing beam voltage. The deeper penetration of electrons into the phosphor results in an increase on the electron–solid interaction volume in which excitation of Ce^{3+} and Pr^{3+} activator ions takes place [21]. Therefore, an increase in interaction volume, which effectively determines the generation of light emission with an increase in electron energy, resulted in an increase

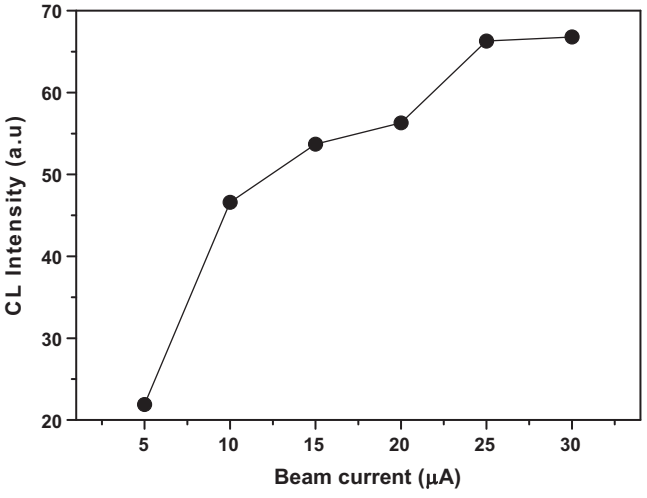

Fig. 9. CL emission intensities of Ce^{3+} in SiO_2: Pr^{3+}–Ce^{3+} phosphor as a function of different beam currents.

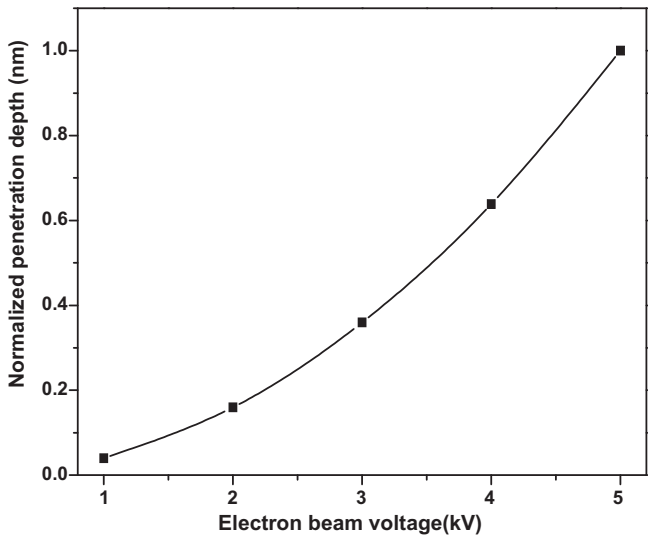

Fig. 10. The calculated penetration depth as a function of electron beam voltage.

in the CL intensity of SiO_2:Pr^{3+}–Ce^{3+}. Furthermore, with an increase of accelerating voltage, more plasmons are being produced by incident electrons resulting in a large number of excited Ce^{3+} and Pr^{3+} ions, thus yielding higher CL intensity [20]. The size of the nanoparticles may, however, play a significant role in the CL intensity at different excitation beam voltages due to the electron excitation volume involved [22], especially when the penetration depth equals the particle size. It is assumed that the CL emission from the boundaries/surface of the nanoparticles is less than that of the inside of the particle due to surface states that may lead to non-radiative decay of the excited electrons.

The CL spectra before and after 50 C/cm^2 electron bombardment are shown in Fig. 11. The CL intensity of the main broad peak at 488 nm with a small shoulder at 450 nm decreased by 80% under 2 keV, 8.5 μA electron beam exposure. Fig. 12 shows the Auger peak-to-peak heights (APPHs) of O and Si elements on the surface of the SiO_2:Pr^{3+}–Ce^{3+} phosphor as a function of electron dose. The CL intensity is plotted on the same figure for comparison. The Auger peak intensity of O was shown to decrease with prolonged electron bombardment of the SiO_2 while that of Si was rather constant. It was also noticed that prolonged electron bombardment led to a

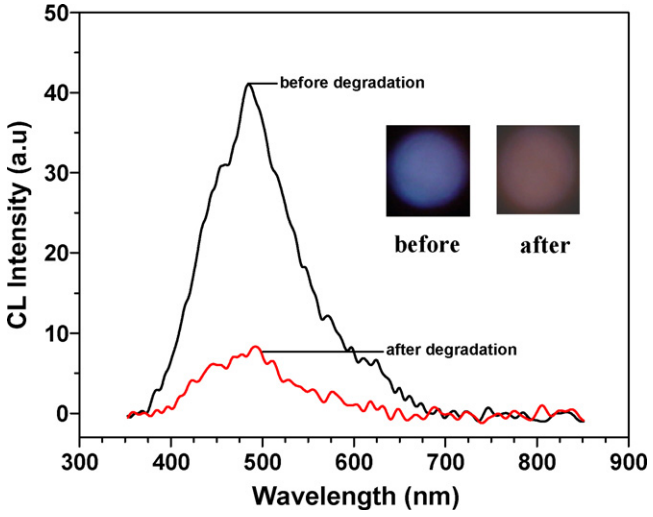

Fig. 11. CL emission spectra of SiO_2:Pr^{3+},Ce^{3+} powder phosphors before and after exposure to 2 keV, 8.5 μA electrons in 1×10^{-7} Torr of O_2 backfilled from the base pressure of 1.2×10^{-8} Torr.

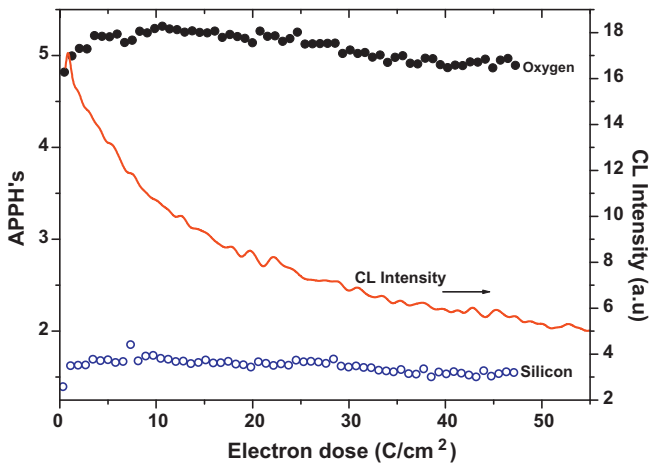

Fig. 12. Auger peak-to-peak heights of O and Si versus 2 keV electron dose at 1×10^{-7} Torr O_2 backfilled from the base pressure of 1.2×10^{-8} Torr.

significant decrease in the CL intensity and this corresponds to the decrease in the Auger peak intensity of O. This correlation between the decrease of CL intensity and that of the Auger peak intensity from O can be attributed to desorption of O from the surface following the electron-beam dissociation of SiO_2 as a result of the formation of an oxygen-deficient surface dead or non-luminescent layer of SiO_x, where $x < 2$ on the surface [23,24]. The colour also changed more to the red region, indicated that the Pr^{3+} is still contributing to the light emission.

4. Conclusion

The CL intensity behaviour of the SiO_2: Pr^{3+}–Ce^{3+} nanophosphor at different concentrations of Ce^{3+} co-doped in SiO_2:Pr^{3+}, beam voltages and beam currents was presented. The CL emission from Ce^{3+} (blue) and Pr^{3+} (red) ions was observed when the concentration of these ions 0.2 mol%, with the blue emission from Ce^{3+} dominating. However, for addition of 1 mol% Ce^{3+} to 0.2 mol% Pr^{3+} led to quenching of Pr^{3+} emission and enhanced blue emission from Ce^{3+} was observed as compared to SiO_2:Ce^{3+}. Energy transfer from Pr^{3+} to Ce^{3+} was discussed. An increase in the CL intensity was observed with increasing beam voltage up to 5 keV and beam current up to 30 μA and no saturation was observed. The CL intensity of the phosphor and Auger peak intensity of O were found to degrade after electron bombardment of the phosphor surface for several hours. Formation of an oxygen-deficient surface dead or non-luminescent layer of SiO_x, where $x < 2$ on the surface is believed to be the main cause of CL degradation of SiO_2:Pr^{3+}–Ce^{3+} nanophosphor.

Acknowledgements

This project is financially supported by the Department of Science and Technology of South Africa and the Council for Scientific and Industrial Research of South Africa.

References

[1] X. Liu, J. Lin, Solid State Sci. 11 (2009) 2030–2036.
[2] S. Tan, P. Yang, C. Li, W. Wang, J. Wang, M. Zhang, X. Jing, J. Lin, Solid State Sci. 12 (2010) 624–629.
[3] H.C. Swart, L. Oosthuizen, P.H. Holloway, G.L.P. Berning, Surf. Interface Anal. 26 (1998) 337–342.
[4] L. Tian, S-I. Mho, Z. Jin, J. Lumin. 129 (2009) 797–800.
[5] Q. Pang, J. Shi, M. Gong, J. Am. Ceram. Soc. 90 (12) (2007) 3943–3946.
[6] O.M. Ntwaeaborwa, H.C. Swart, R.E. Kroon, J.M. Ngaruiya, J.R. Botha, P.H. Holloway, Photoluminescence Research Progress, Nova Science Publishers, 2008, pp. 287–306, ISBN: 987-1-60456-538-6, Chapter 11.

[7] G. Lakshminarayana, J. Qiu, M.G. Brik, I.V. Kityk, J. Phys. D: Appl. Phys. 41 (2008) 175106.
[8] Q.Y. Zhang, X.Y. Huang, Progr. Mater. Sci. 55 (2010) 353–427.
[9] G. Blasse, B.C. Grabmaier, Luminescent Materials, Springer-Verlag, Berlin, 1994.
[10] H.B. Tripathi, A.K. Agarwal, H.C. Kandpal, R. Belwal, Solid State Commun. 28 (1978) 807–814.
[11] I. Prakash, P Muralidharan, N. Nallamuthu, N. Satyanarayana, J. Am. Ceram. Soc. 89 (7) (2006) 2220–2225.
[12] M. Fasoli, A. Vedda, A. Lauria, F. Moretti, E. Rizzelli, N. Chiodini, F. Meunardi, M. Nikl, J. Non-Cryst. Solids 355 (2009) 1140–1144.
[13] G. De, D. Kundu, B. Karmakar, D. Ganguli, J. Non-Cryst. Solids 155 (1993) 253–258.
[14] H. Yoshino, K. Kamiya, H. Nasu, J. Non-Cryst. Solids 126 (1990) 68–78.
[15] H.S. Jang, W.B. Im, D.C. Lee, D.Y. Jeon, S.S. Kim, J. Lumin. 126 (2007) 371–377.
[16] Z. Nie, K-S. Lim, J. Zhang, X. Wang, J. Lumin. 129 (2009) 844–849.
[17] P. Vergeer, V. Babin, A. Meijerink, J. Lumin. 114 (2005) 267–274.
[18] A. Meijerink, R. Wegh, P. Vergeer, T. Vlugt, Opt. Mater. 28 (2006) 575–581.
[19] L.F. Koao, H.C. Swart, E. Coetsee, M.M. Biggs, F.B. Dejene, Phys. B: Phys. Condens. Matter 404 (2009) 4499–4503.
[20] X. Liu, J. Lin, J. Nanoparticle Res. 9 (2007) 869–875.
[21] C. Lin, H. Wang, D. Kong, M. Yu, X. Liu, Z. Wang, J. Lin, Eur. J. Inorg. Chem. (2006) 3667–3675.
[22] K. Vinay, M. Varun, S.P. Shreyas, I.M. Nagpure, E. Coetsee, O.M. Ntwaeaborwa, H.C. Swart, J. Appl. Phys. 107 (12) (2010) 123533.
[23] G.H. Mhlongo, O.M. Ntwaeaborwa, M.S. Dhlamini, H.C. Swart, K.T. Hillie, J Mater. Sci. 45 (2010) 5228–5236.
[24] O.M. Ntwaeaborwa, H.C. Swart, R.E. Kroon, P.H. Holloway, J.R. Botha, J. Phys. Chem. Solids 67 (2006) 1749–1753.